New Perspectives on Iron–Ligand Vibrations of Oxyheme Complexes[**]

Supporting Information

Jianfeng Li, Qian Peng, Alexander Barabanchikov, Jeffrey W. Pavlik, E. Ercan Alp, Wolfgang Sturhahn, Jiyong Zhao, Charles E. Schulz, J. Timothy Sage and W. Robert Scheidt[*]

May 3, 2011

[☆] Dr. Jianfeng Li, Dr. Qian Peng, Jeffrey W. Pavlik, Prof. W. Robert Scheidt
Department of Chemistry and Biochemistry
University of Notre Dame, Notre Dame, Indiana 46556 (USA)
Fax (574) 631-6652
E-mail: Scheidt.1@nd.edu

Dr. Alexander Barabanschikov, Prof. J. Timothy Sage
Department of Physics and Center for Interdisciplinary Research on Complex Systems,
Northeastern University, Boston, Massachusetts 02115 (USA)
E-mail: jtsage@neu.edu

Dr. E. Ercan Alp, Dr. Wolfgang Sturhahn, Dr. Jiyong Zhao
Advanced Photon Source, Argonne National Laboratory
Argonne, Illinois 60439 (USA)

Prof. Charles E. Schulz
Department of Physics, Knox College
Galesburg, Illinois 61401 (USA)

[☆☆] We thank the National Institutes of Health for support of this research under Grant GM-38401 to WRS and the NSF under PHY-0545787 to JTS. Use of the Advanced Photon Source, an Office of Science User Facility operated for the US Department of Energy (DOE) Office of Science by Argonne National Laboratory, was supported by the U.S. DOE under Contract No. DE-AC02-06CH11357.

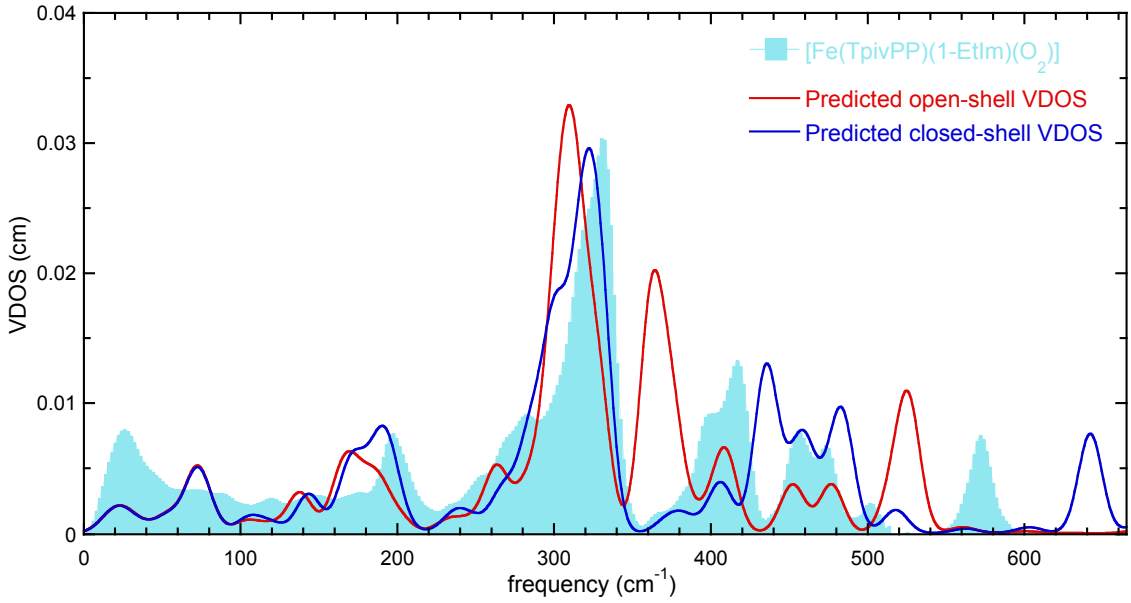

Figure S1. Comparison of the observed powder spectrum of [Fe(TpivPP)(1-EtIm)(O_2)] (filled blue) with the DFT predicted spectrum of the closed shell singlet (blue line) and the DFT predicted spectrum of the open shell singlet (red line).

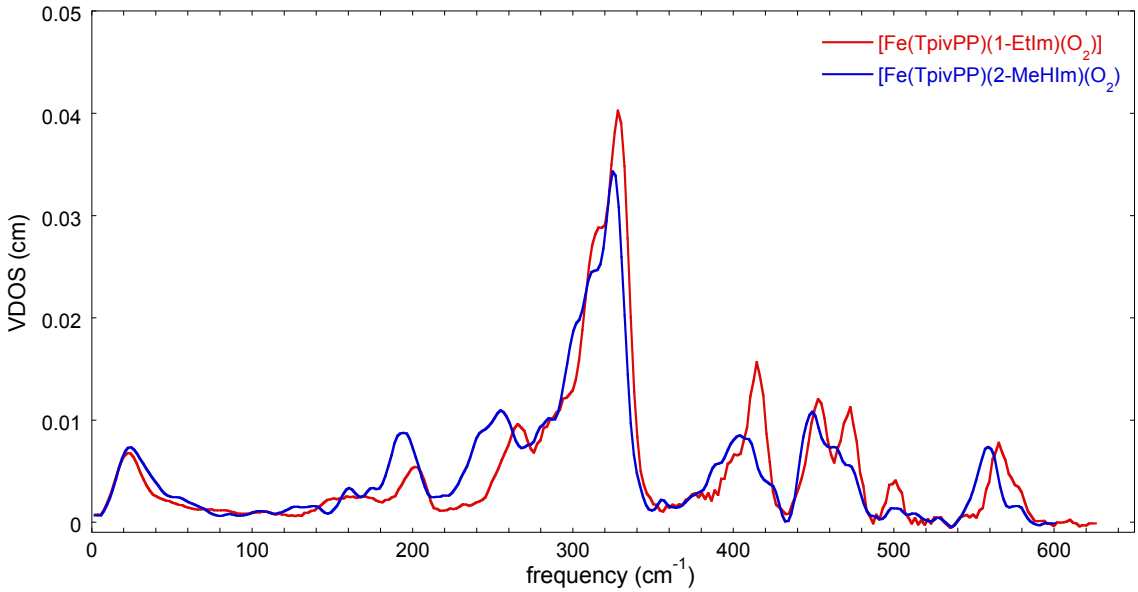

Figure S2. The measured in-plane VDOS for [Fe(TpivPP)(2-MeHIm)(O_2)] and [Fe(TpivPP)(1-EtIm)(O_2)]. The in-plane spectrum was taken with the porphyrin plane oriented parallel to the excitation beam.

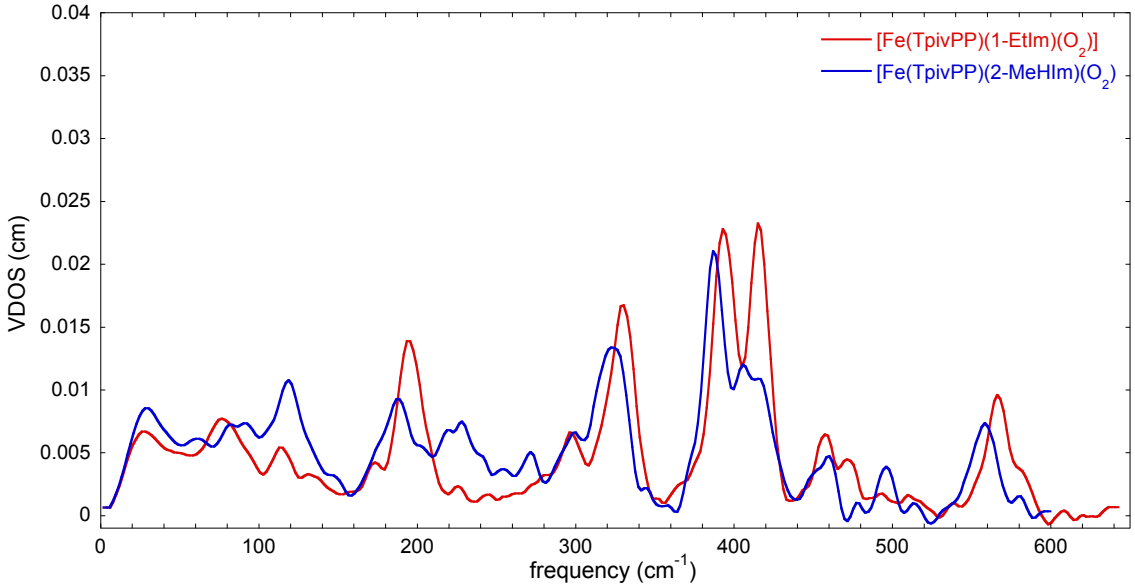

Figure S3. The measured out-of-plane VDOS for [Fe(TpivPP)(2-MeHIm)(O_2)] and [Fe(TpivPP)(1-EtIm)(O_2)]. The out-of-plane spectra were taken with the porphyrin plane oriented perpendicular to the excitation beam.

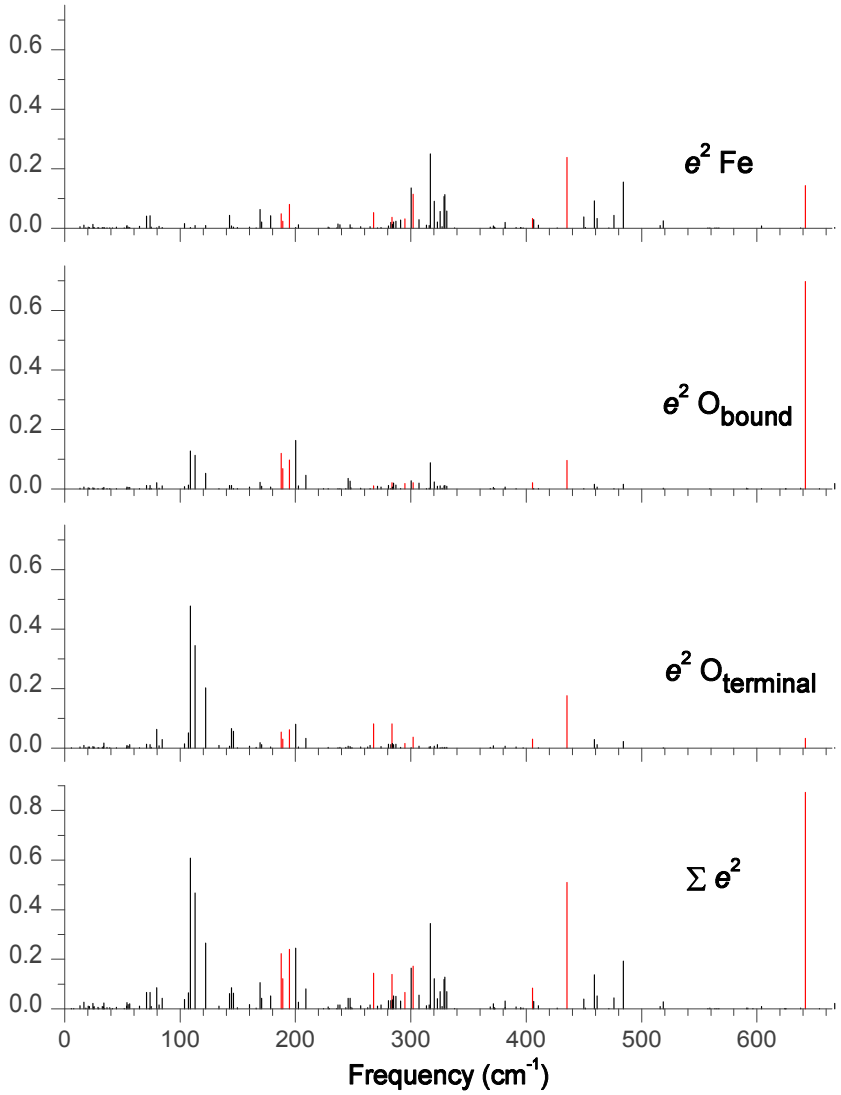

Figure S4. The predicted vibrational kinetic energy distributions over the Fe–O_2 fragment in [Fe(TpivPP)(1-EtIm)(O_2)]. The heights of the individual bars equal the fraction of the kinetic energy associated with each atom or group. The lower panel shows the sum of the mode composition factors for Fe, O_{bound}, and $O_{terminal}$, and gives the fraction of mode energy localized on the Fe–O_2 fragment. Red bars indicate Fe–O_2 modes.

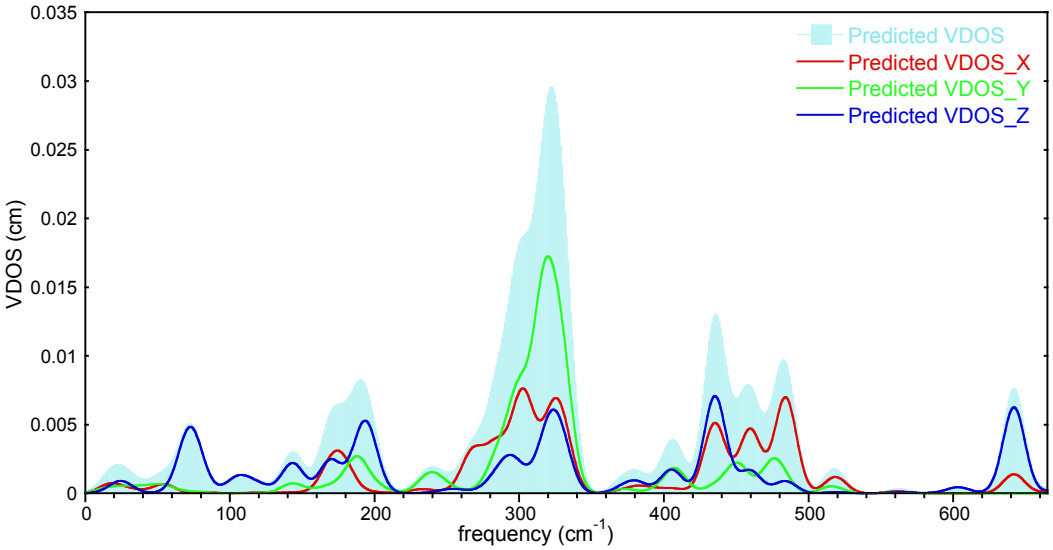

Figure S5. The predicted VDOS for [Fe(TpivPP)(1-EtIm)(O_2)] displaying the predicted anisotropy in the vibrational spectrum for the observed orientation of O_2 and imidazole. The color code for the plot shows the projection of iron motion along z (perpendicular to porphyrin plane, blue), x (along the Fe–O_2 plane, red) and y (perpendicular to the Fe–O_2 plane, green).

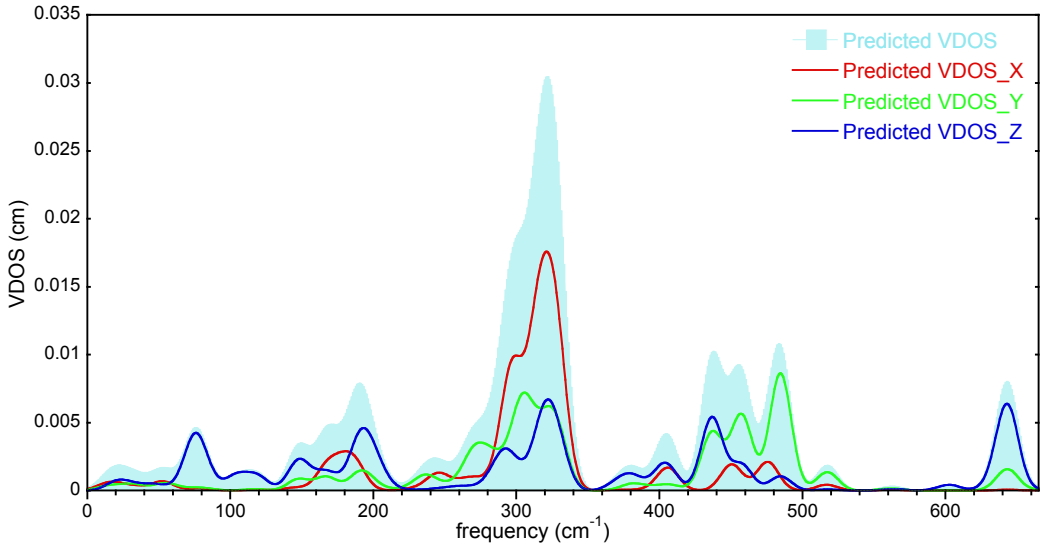

Figure S6. The predicted VDOS for [Fe(TpivPP)(1-EtIm)(O_2)] displaying the anisotropy in the vibrational spectrum; after rotation of the Fe–O_2 plane by 90° holding all else constant. The color code for the plot shows the projection of iron motion along z (perpendicular to porphyrin plane, dark blue), x (perpendicular to the Fe–O_2 plane, red) and y (parallel to the Fe–O_2 plane, green). The Fe–O_2 and imidazole planes are chosen to be coplanar and bisecting two opposite N–Fe–N angles.

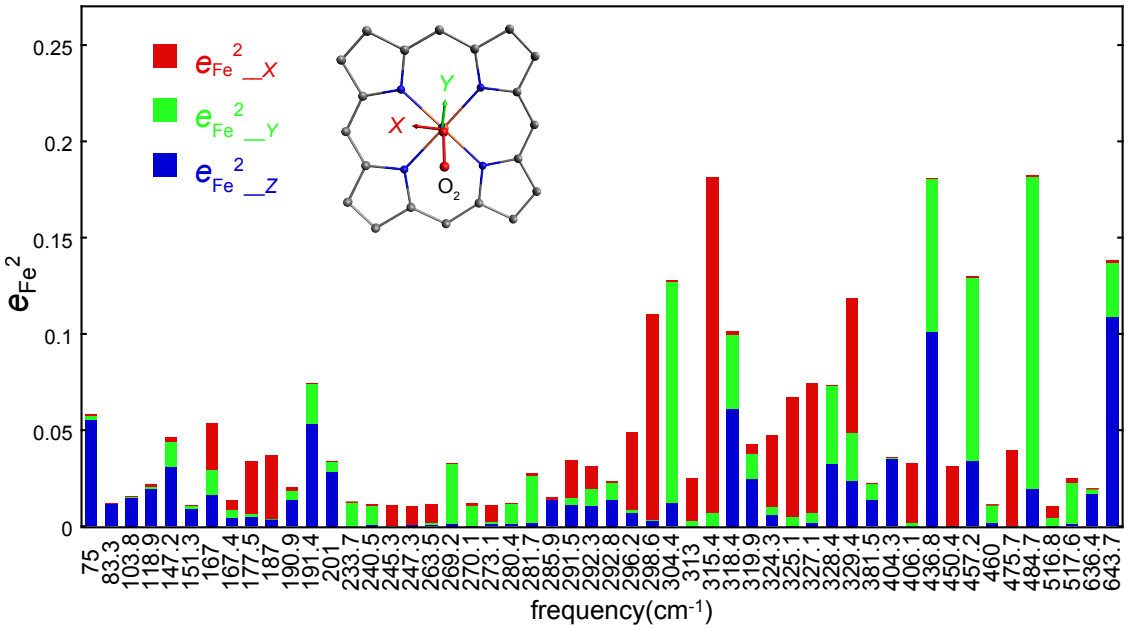

Figure S7. The predicted directional characteristics of all modes with $e^2_{Fe} > 0.01$ for the idealized structure in which the Fe–O_2 and imidazole planes were required to be coplanar. The values of the predicted frequencies are given at each tick mark, but the horizontal scale is only approximately linear in frequency to avoid overlaps. The color code for the plot shows the projection of iron motion along z (perpendicular to porphyrin plane, blue), x (perpendicular to the Fe–O_2 projection, red) and y (along the Fe–O_2 projection, green). Note that although the relative orientation of the Fe–O_2 plane has changed, we retain the same coordinate system and color scheme as in Figure 5 (main text) to facilitate comparisons.

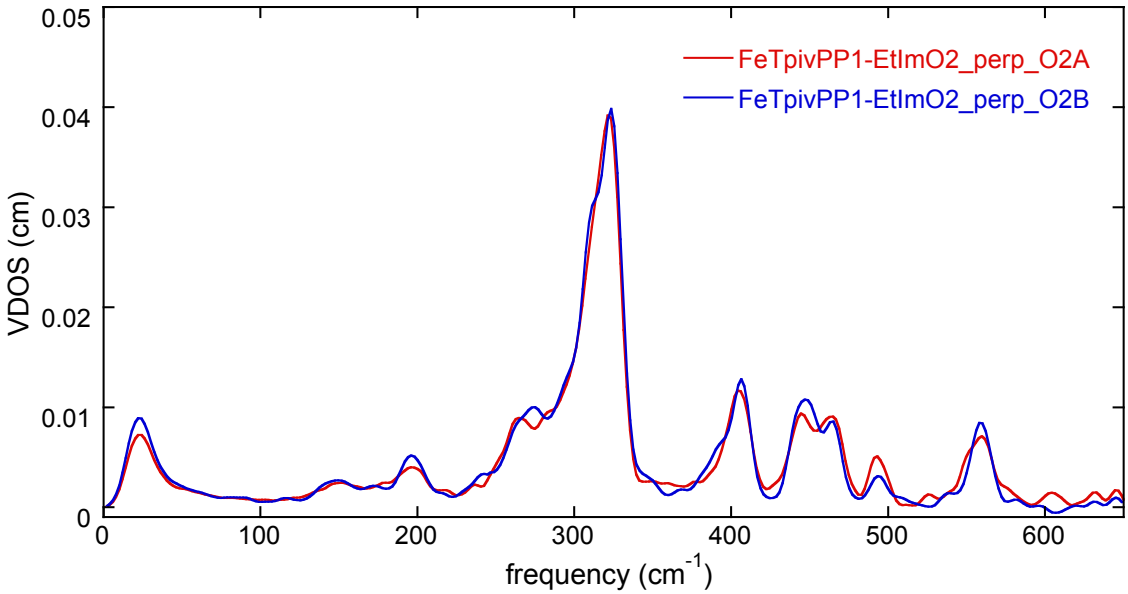

Figure S8. Experimental in-plane spectra taken in the direction perpendicular to the two nearly orthogonal Fe-O_2 orientations in [Fe(TpivPP)(1-EtIm)(O_2)].

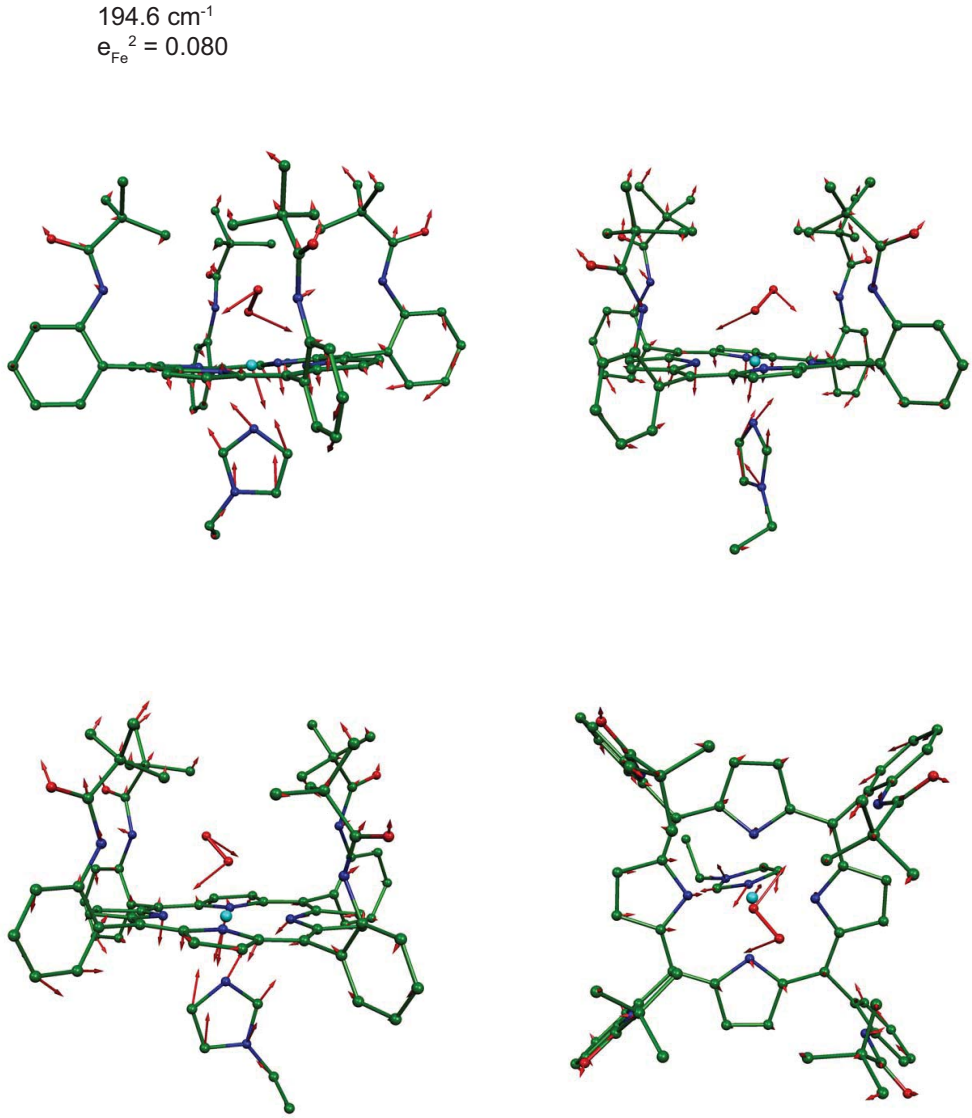

Figure S9. Edge and top views of the predicted 195 cm^{-1} mode of [Fe(TpivPP)(1-EtIm)(O_2)].

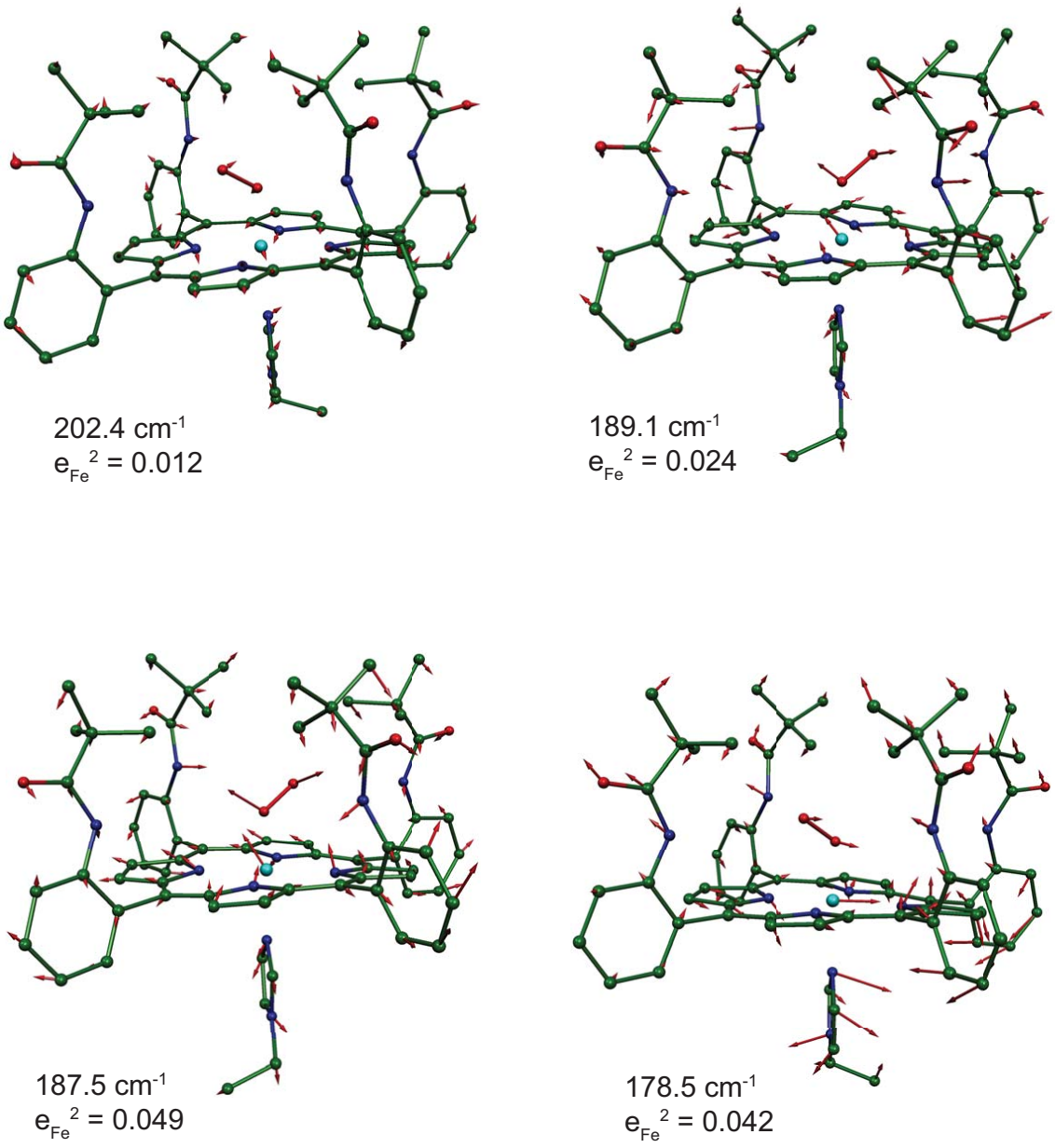

Figure S10. The predicted vibrational modes of [Fe(TpivPP)(1-EtIm)(O_2)] in the region from 202 cm^{-1} to 70 cm^{-1}.

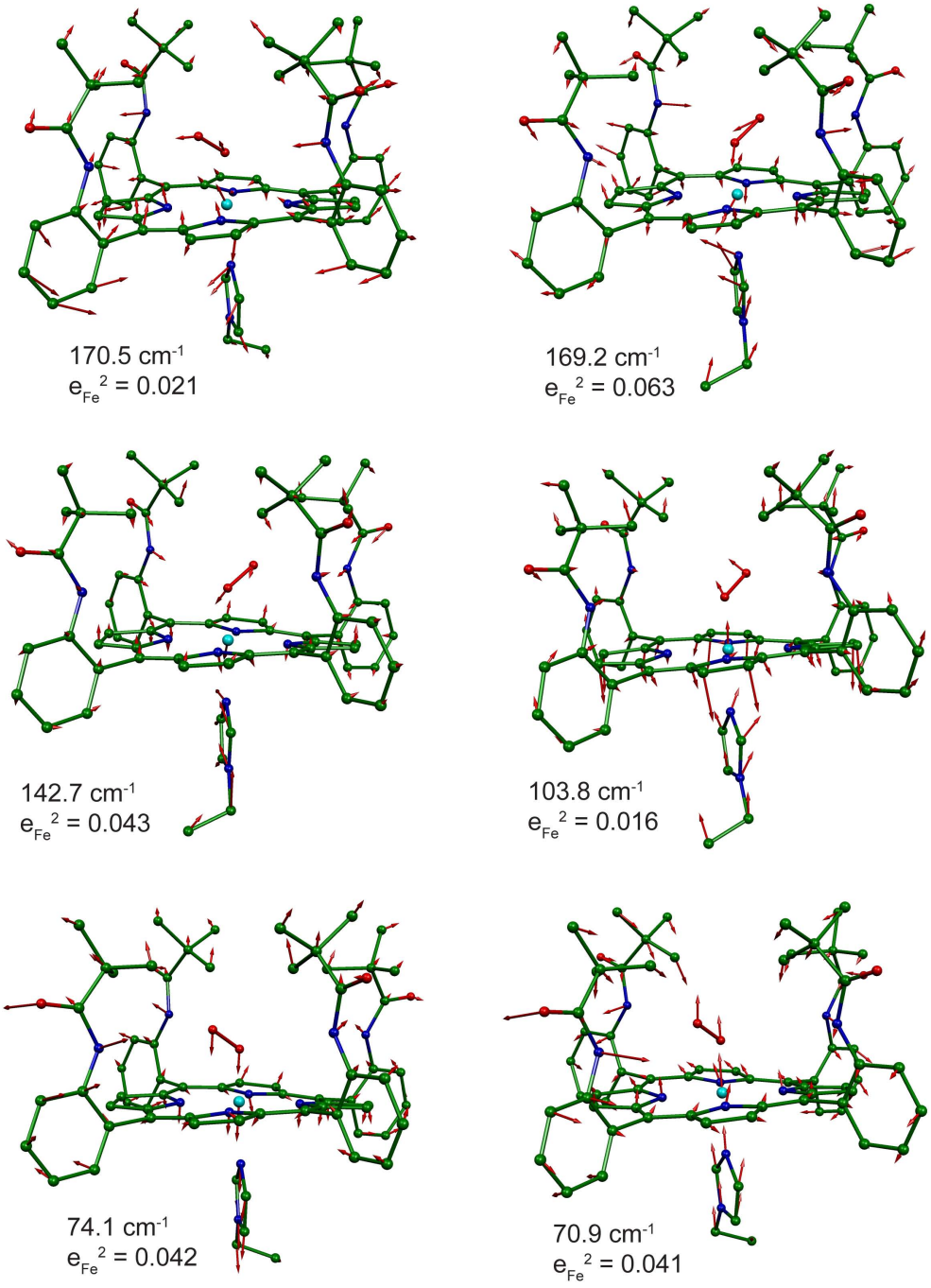

Figure S10. Continued.

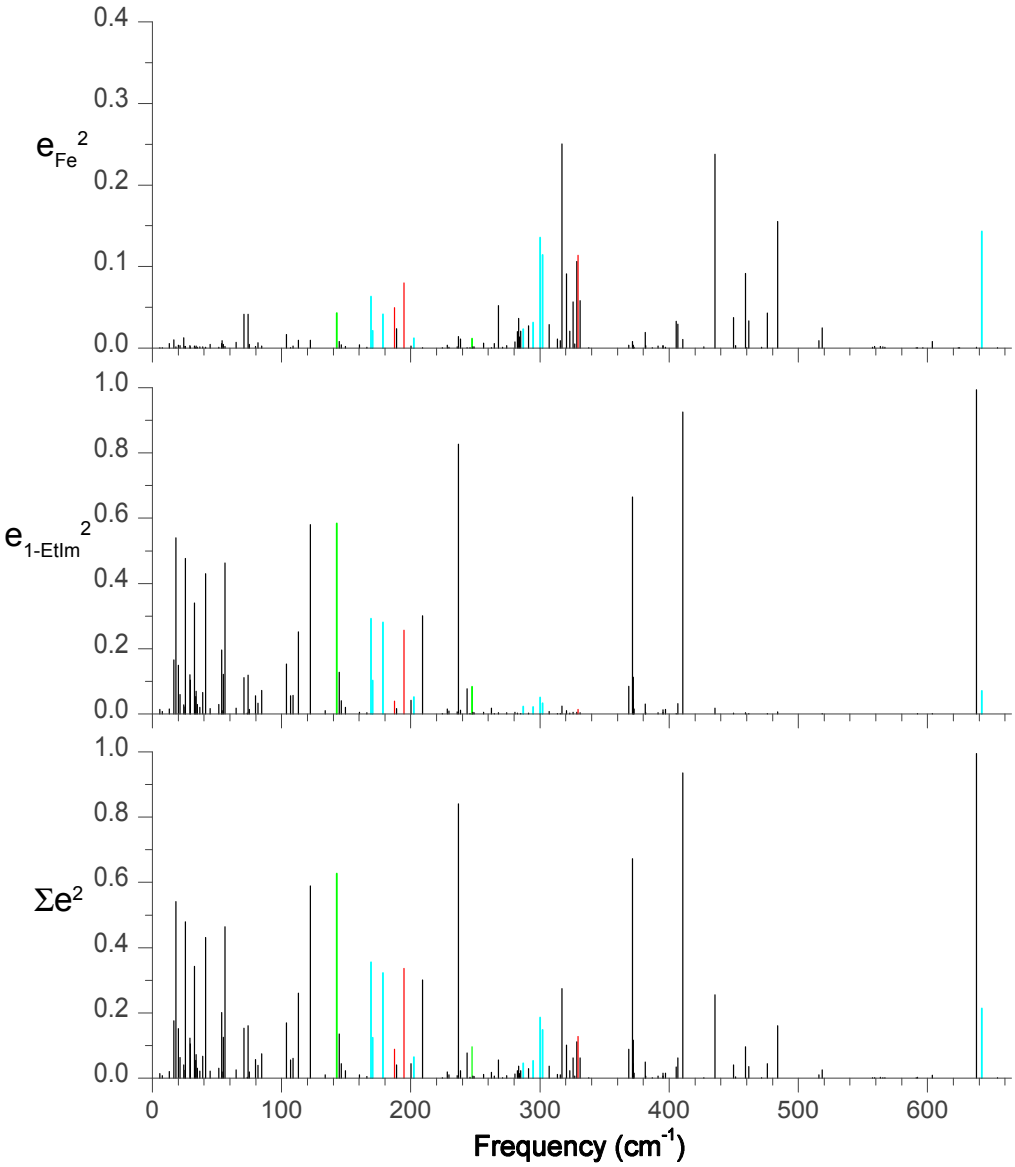

Figure S11. The predicted vibrational kinetic energy distributions of the Fe–1-EtIm fragment (which includes all 15 atoms of the 1-EtIm group) in [Fe(TpivPP)(1-EtIm)(O_2)]. The height of the individual bars equals the fraction of the kinetic energy associated with each atom or group. The lower panel shows the sum of the mode composition factors for Fe and 1-EtIm, and gives the fraction of mode energy localized on the Fe–1-EtIm fragment. Note the $e_{Fe}{}^2$ plot is on a different scale. Modes that involve simultaneously Fe and 1-EtIm motions are colored. Red and light blue bars indicate Fe–1-EtIm translation modes with 1-EtIm movement parallel or perpendicular to Fe–N_{Im} vector respectively; green bars indicate modes with strong imidazole rotation as well as Fe–Im stretch.

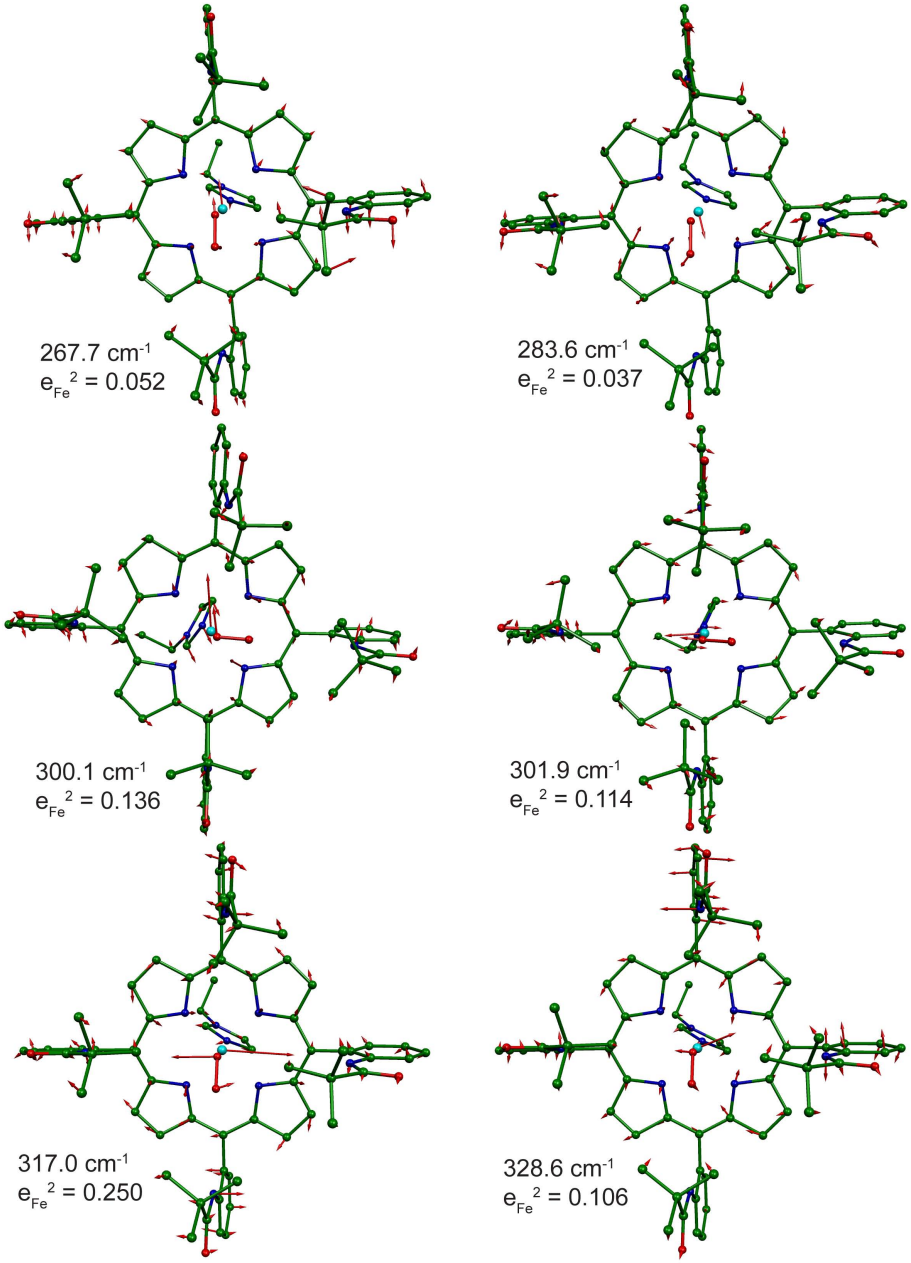

Figure S12. The predicted in-plane modes of [Fe(TpivPP)(1-EtIm)(O_2)] in the frequency range of 260–330 cm^{-1}. Note the direction of iron motion relative the the orientation of the Fe–O_2 plane.

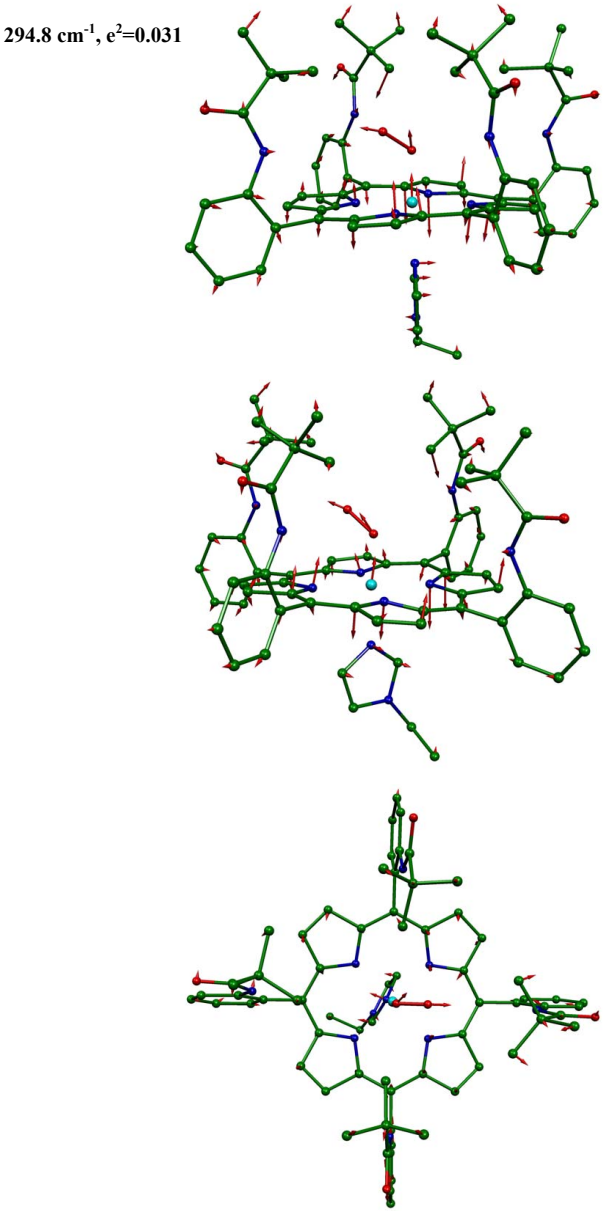

Figure S13. The predicted character of the band observed at 296 cm^{-1}.

Table S1. *x, y, z* components of iron energy for normal modes with total iron energy above 0.01 of [Fe(TpivPP)(1-EtIm)(O_2)]. (optimized on a structure with the Fe--O--O plane near-perpendicular to imidazole plane).

Mode(cm^{-1})	e^2_x	e^2_y	e^2_z	e^2
16.6	0.009	0.000	0.000	0.010
24.4	0.000	0.001	0.011	0.013
70.9	0.000	0.000	0.041	0.041
74.1	0.000	0.001	0.041	0.042
103.8	0.000	0.000	0.016	0.016
142.7	0.001	0.012	0.030	0.043
169.2	0.026	0.006	0.032	0.063
170.5	0.008	0.001	0.013	0.021
178.5	0.036	0.005	0.000	0.042
187.5	0.001	0.031	0.018	0.049
189.1	0.001	0.016	0.007	0.024
194.6	0.000	0.001	0.079	0.080
202.4	0.000	0.008	0.004	0.012
236.8	0.002	0.012	0.000	0.014
238.5	0.000	0.011	0.000	0.011
247.4	0.001	0.010	0.001	0.012
267.7	0.051	0.002	0.000	0.052
282.5	0.010	0.010	0.000	0.020
283.6	0.027	0.006	0.004	0.037
284.1	0.008	0.003	0.002	0.014
285.0	0.002	0.018	0.001	0.021
287.1	0.015	0.001	0.007	0.023
291.2	0.000	0.020	0.007	0.027
294.8	0.000	0.000	0.031	0.031
300.1	0.013	0.122	0.000	0.136
301.9	0.103	0.001	0.010	0.114
307.2	0.025	0.000	0.004	0.029
313.6	0.000	0.010	0.001	0.011
317.0	0.001	0.234	0.015	0.250
320.4	0.043	0.001	0.048	0.091
323.0	0.012	0.007	0.002	0.021
325.5	0.029	0.000	0.028	0.057
328.6	0.024	0.078	0.004	0.106
329.4	0.007	0.090	0.017	0.114
331.1	0.034	0.004	0.021	0.058
381.6	0.007	0.001	0.012	0.019
405.4	0.003	0.000	0.030	0.033
406.6	0.001	0.026	0.002	0.029
410.7	0.002	0.008	0.000	0.011
435.3	0.095	0.010	0.133	0.238
449.9	0.000	0.037	0.000	0.038
459.0	0.065	0.003	0.024	0.091

461.5	0.023	0.003	0.007	0.033
475.9	0.001	0.043	0.000	0.043
484.1	0.131	0.008	0.017	0.155
518.6	0.023	0.000	0.002	0.025
642.0	0.026	0.000	0.117	0.143
677.3	0.009	0.000	0.004	0.013

Table S2. *x, y, z* components of iron energy for normal modes with total iron energy above 0.01 of [Fe(TpivPP)(1-EtIm)(O_2)] (optimized on a structure with the Fe--! ""O plane near-coplanar to imidazole plane).

Mode(cm^{-1})	e^2_x	e^2_y	e^2_z	e^2
75.0	0.001	0.002	0.056	0.058
83.3	0.000	0.000	0.012	0.012
103.8	0.000	0.000	0.015	0.015
118.9	0.001	0.001	0.020	0.022
147.2	0.002	0.013	0.031	0.046
151.3	0.001	0.001	0.009	0.011
167.0	0.024	0.013	0.016	0.053
167.4	0.005	0.004	0.005	0.013
177.5	0.027	0.002	0.005	0.034
187.0	0.033	0.000	0.004	0.037
190.9	0.002	0.005	0.014	0.020
191.4	0.000	0.020	0.053	0.074
201.0	0.000	0.006	0.028	0.034
233.7	0.000	0.013	0.000	0.013
240.5	0.001	0.010	0.001	0.012
245.3	0.011	0.000	0.000	0.011
247.3	0.010	0.000	0.001	0.011
263.5	0.010	0.001	0.001	0.011
269.2	0.000	0.031	0.001	0.033
270.1	0.001	0.011	0.000	0.012
273.1	0.009	0.001	0.001	0.011
280.4	0.000	0.010	0.002	0.012
281.7	0.001	0.024	0.002	0.027
285.9	0.001	0.001	0.014	0.015
291.5	0.020	0.004	0.011	0.034
292.3	0.012	0.009	0.011	0.031
292.8	0.001	0.009	0.014	0.023
296.2	0.040	0.002	0.007	0.049
298.6	0.107	0.000	0.003	0.110
304.4	0.001	0.115	0.012	0.128
313.0	0.022	0.003	0.000	0.025
315.4	0.174	0.007	0.000	0.181
318.4	0.002	0.039	0.061	0.102
319.9	0.005	0.013	0.025	0.043
324.3	0.037	0.004	0.006	0.047

325.1	0.062	0.005	0.000	0.067
327.1	0.067	0.005	0.002	0.075
328.4	0.000	0.040	0.033	0.073
329.4	0.070	0.025	0.024	0.119
381.5	0.000	0.008	0.014	0.022
404.3	0.000	0.000	0.035	0.036
406.1	0.031	0.002	0.000	0.033
436.8	0.000	0.080	0.101	0.181
450.4	0.031	0.000	0.000	0.031
457.2	0.001	0.095	0.034	0.130
460.0	0.000	0.009	0.002	0.011
475.7	0.039	0.000	0.000	0.040
484.7	0.001	0.162	0.020	0.182
516.8	0.006	0.004	0.000	0.010
517.6	0.002	0.021	0.002	0.025
636.4	0.000	0.003	0.017	0.020
643.7	0.001	0.028	0.109	0.138

Table S3. *x, y, z* components of iron energy for normal modes with total iron energy above 0.01 of [Fe(TpivPP)(2-MeHIm)(O_2)] (optimized on a structure with the Fe--O--O plane near-perpendicular to imidazole plane).

Mode(cm^{-1})	e^2_x	e^2_y	e^2_z	e^2
23.1	0.001	0.000	0.011	0.012
54.7	0.008	0.004	0.000	0.012
74.9	0.000	0.000	0.034	0.035
77.5	0.001	0.000	0.051	0.052
106.6	0.000	0.000	0.019	0.019
112.2	0.000	0.001	0.020	0.021
148.0	0.001	0.009	0.006	0.016
155.4	0.034	0.000	0.018	0.052
158.8	0.006	0.001	0.080	0.086
160.8	0.002	0.003	0.041	0.045
170.5	0.000	0.013	0.005	0.019
185.5	0.000	0.004	0.059	0.063
195.5	0.000	0.031	0.002	0.033
199.4	0.023	0.000	0.003	0.027
203.6	0.000	0.011	0.001	0.011
248.0	0.000	0.011	0.000	0.011
261.8	0.014	0.002	0.002	0.018
271.9	0.034	0.000	0.003	0.036
278.3	0.002	0.002	0.020	0.023
285.5	0.012	0.006	0.001	0.019
289.5	0.018	0.000	0.008	0.026
292.8	0.013	0.006	0.001	0.020
296.4	0.004	0.000	0.023	0.027
299.5	0.028	0.097	0.001	0.126

304.2	0.083	0.026	0.003	0.112
313.7	0.002	0.007	0.002	0.011
315.8	0.008	0.011	0.002	0.022
318.2	0.002	0.135	0.002	0.139
319.9	0.042	0.002	0.045	0.089
324.9	0.027	0.017	0.012	0.056
325.4	0.030	0.083	0.005	0.118
326.6	0.030	0.000	0.007	0.037
329.3	0.032	0.044	0.018	0.094
331.8	0.027	0.000	0.010	0.038
332.3	0.002	0.162	0.000	0.164
383.1	0.007	0.001	0.005	0.013
399.8	0.001	0.013	0.001	0.015
408.9	0.004	0.001	0.030	0.035
409.7	0.001	0.041	0.001	0.042
436.0	0.080	0.001	0.131	0.212
450.1	0.000	0.004	0.010	0.014
450.8	0.000	0.039	0.002	0.041
458.0	0.082	0.001	0.037	0.120
476.5	0.000	0.045	0.000	0.045
484.3	0.132	0.001	0.024	0.157
519.0	0.026	0.000	0.003	0.029
643.6	0.008	0.000	0.046	0.055
652.2	0.025	0.000	0.061	0.086